

**EVIDENCE OF SUBSTRUCTURE IN
THE CLUSTER OF GALAXIES A3558**

Christine C. Dantas¹

Reinaldo R. de Carvalho^{2,3}

Hugo V. Capelato¹

Alain Mazure⁴

Received ——— ; accepted ———

Submitted to ApJ.

¹Divisão de Astrofísica, INPE/MCT, CP 515, S. J. dos Campos, SP 12201-970, Brazil.

²Present address: Caltech - Astronomy Dept., Pasadena, CA 91125, USA.

³On leave of absence from Observatório Nacional/CNPq, DAF, Brazil.

⁴IGRAP/LAS Traverse du Siphon 13012, Marseille, France.

ABSTRACT

We investigate the dynamical properties of the cluster of galaxies A3558 (Shapley 8). Studying a region of one square degree ($\sim 3 \text{ Mpc}^2$) centered on the cluster cD galaxy, we have obtained a statistically complete photometric catalog with positions and magnitudes of 1421 galaxies (down to a limiting magnitude of $B \sim 21$). This catalog has been matched to the recent velocity data obtained by Mazure et al. (1997) and from the literature, yielding a radial velocity catalog containing 322 galaxies. We analyse the resulting catalog in search of substructure, using different statistical techniques. This analysis shows that the position/velocity space distribution of galaxies shows significant substructure.

A central bimodal core detected previously in a preliminary study (Dantas, de Carvalho & Capelato 1994) and by an analysis of the X-ray emission map (Slezak et al. 1994) is confirmed using the Adaptive Kernel Technique and Wavelet Analysis. We show that this central bimodal substructure is nevertheless composed of a projected feature, kinematically unrelated to the cluster, plus a group of galaxies probably in its initial merging phase into a relaxed core. The cD velocity offset with respect to the average cluster redshift, reported earlier by several authors, is completely eliminated as a result of our dynamical analysis. The untangling of the relaxed core component also allows a better, more reliable determination of the central velocity dispersion, which in turn eliminates the “ β -problem” for A3558. The cluster also shows a “preferential” distribution of subclumps coinciding with the direction of the major axis position angle of the cD galaxy and of the central X-ray emission ellipsoidal distribution, in agreement with the anisotropic merger scenario described by West (1994a).

Subject headings: galaxies: clusters: individual (A3558) — galaxies: clusters:

general — catalogs — cosmology: observations

1. Introduction

Clusters of galaxies stand as the ideal probes to test the presently accepted hierarchical scenario of structure formation. According to this picture, if $\Omega \sim 1$, rich clusters are still being formed by mergers of individual groups of galaxies from the field (Richstone et al. 1992). Recent optical and X-ray observations seem to be in agreement with that hypothesis, since substructure is found in a large fraction of clusters ($\sim 40\text{--}75\%$, see Bird 1994, West 1994b and references therein). Recent simulations (e.g. Katz & White 1993) based on the hierarchical scenario are also beginning to show features with properties that can be associated to substructures found in real clusters.

Apart from the cosmological point of view, the complexity of the multicomponent environment (gas, galaxies and dark matter) which constitutes a cluster of galaxies can provide important clues to the formation and evolution of individual galaxies. It is specially important to investigate these structural and evolutionary trends within substructures, where galaxy alterations (morphological type, size, and mass distribution) within the denser substructure environment might be more clearly untangled (e.g. Whitmore 1990).

There are several statistical techniques now available to quantify substructures in clusters. One of the first systematic works was carried out by Geller & Beers (1982). Using only 2-D projected data, they found that $\sim 40\%$ of the clusters in their sample show statistically significant substructures. Later, Dressler & Shectman (1988) developed a statistic based on both position and velocity information, and found similar results when applying their test to a sample of 15 clusters. However, in a subsequent study, West & Bothun (1990) reached opposite conclusions. Bird (1994) have analysed the several proposed methods and statistics in detail and concluded that $\sim 50\%$ of the studied sample (33 clusters) contains substructures. More recently, Kriessler & Beers (1997) constructed new 2-D contour maps using Dressler's (1980) sample (the same sample analysed previously

by Geller & Beers 1982). By the application of the Adaptive Kernel technique (Silverman 1986), they found that 57 % of clusters in their sample presented significant substructure.

The goal of this work is to investigate the structural and dynamical properties of the individual cluster of galaxies A3558 (Shapley 8), in terms of substructure analysis. This cluster has been an object of extensive optical and X-ray observations in the past few years (e.g. Metcalfe et al. 1987, Teague et al. 1990, Bardelli et al. 1993, Bardelli et al. 1996, Markevitch, Sarazin, & Henriksen 1996, Dantas, de Carvalho & Capelato 1994, Dantas 1996). This cluster, classified as richness class 4 in the ACO catalog (Abell, Corwin & Olowin 1989) and dominated by a central giant cD galaxy, has attracted much interest, first, due to its location - at the core of the Shapley Concentration, a supercluster composed of 25 clusters of galaxies and rich in X-ray emitting clusters (e.g. Raychaudhury et al. 1991, Zucca et al. 1993), and second, because of its dynamical complexity due to the presence of substructure (e.g. Bardelli et al. 1996).

Some authors have reported that the central cD galaxy of A3558 has a peculiar velocity relative to the cluster average velocity (Gebhardt & Beers 1991). This “offset”, also found in several cD clusters, was shown by Bird (1994) to be strongly correlated to the presence of substructure in the cluster. Using the KMM method (e.g. Ashman, Bird & Zepf 1995), in order to assign galaxies to their most probable substructure, she concluded that the velocity offset remained only in 2 out of 25 analysed clusters (including A3558). Later on, Bardelli et al. (1996) partitioned his A3558 velocity sample into two sub-samples and verified that the cD velocity was consistent with the average velocity of one of the subsamples, but the detailed relation of the original offset to the nature of the dynamical status of the central core was never cleared.

Also, one more component of uncertainty in A3558 is its apparently “extreme” β -discrepancy, as described by Bardelli et al., which could not be accounted for using the

proposed correction of Bahcall & Lubin (1993). The β -problem, first noted by Gorenstein et al. (1978) and Jones & Forman (1984), can be stated in its simple version (see details in e.g. Gerbal et al. 1994) as an incompatibility between the observed X-ray slope of the hot intracluster gas and the theoretical temperature ratio of galaxies to gas. This problem has often been referred to in the literature, and some solutions have been proposed (e.g. Bahcall & Lubin 1994, Gerbal et al. 1994).

In this paper, we resolve the cD offset and the β -problem in A3558, using a careful and detailed substructure analysis of a statistically complete velocity sample of galaxies. We present the data reduction and methodology in Section 2. In Section 3, we briefly review the current available statistical techniques to look for substructure and apply them to A3558 in Section 4. In Section 5, we discuss the results and a comparison of all the methods and their significance. We use $q_0 = 0.1$ and $H_0 = 75 \text{ km s}^{-1} \text{ Mpc}^{-1}$ throughout.

2. Data Reduction and Methodology

2.1. Data

The Abell cluster A3558 (Shapley 8) has been extensively observed in the last five years (e.g. Bardelli et al. 1993). It is at a distance of $\sim 14400 \text{ km s}^{-1}$ and is located at the core of the Shapley Concentration, a supercluster composed of 25 clusters of galaxies. This cluster is classified as richness class 4 in the ACO catalog (Abell, Corwin & Olowin 1989), and is dominated by a central giant cD galaxy. The cluster seems to be relatively rich in elliptical/lenticular galaxies (Metcalf et al. 1994). All this is suggestive of a regular and well relaxed rich cluster of galaxies. We explore this hypothesis by analysing both the projected distribution of galaxies as well as its velocity field. Extensive spectroscopic surveys of clusters of galaxies (e.g. the ESO surveys, ENACS, the Canadian CNOC survey)

have been carried out recently. However, a well defined magnitude limited catalog is of fundamental importance for a follow-up spectroscopic study, so that the investigation of the physical properties of clusters becomes meaningful.

We have obtained two digitized images of A3558: one with resolution of 1.67 arcsec/pixel and the other with 1 arcsec/pixel (Lasker et al. 1990), through scans of the deep IIIa-J plates available at STScI⁵. Measurement of photometric attributes are improved by the use of high resolution images, but the noise contribution proportionally increases in the scanning process. For this reason, we tested the confidence limits of the final photometric catalog by analysing both images of A3558 (defined by a field of $1^\circ \times 1^\circ$, centered on the cD galaxy).

2.2. Detection and Classification With FOCAS

The data reduction was performed using the FOCAS package (Valdes 1982). Several tests were carried out for both images and for a simulated cluster image in order to understand how the output catalog responded to variations in the object detection parameters (Dantas 1996). These tests show that the 1 arcsec/pixel resolution image provided a higher quality information, being a compromise between noiser measurement and better sampling. We defined a minimum detection area of 65 px², corresponding to the area of a circle with radius equal to ~ 3 times the typical seeing disc at Siding Spring. Detection was performed at a threshold level of 3 times the sky rms. This corresponds on average to 7 % of the local sky value. Besides the detection procedure, an important step

⁵Photometry obtained using the Guide Stars Selection System Astrometric Support Program developed at the Space Telescope Science Institute (STScI is operated by the Association of Universities for Research in Astronomy, Inc., for NASA).

in building a reliable catalog is to set the “Point Spread Function” (PSF) which is to be used in the object classification procedure. A specific program in FOCAS automatically searches for stellar and non-saturated objects for the construction of the PSF. In this work, we limited that search for stars to the magnitude interval of B $16^m - 19^m$. The stars selected by FOCAS were visually inspected and after pruning asymmetric objects we then recomputed the PSF. The classification of objects was then performed according to specific rules in FOCAS that we kept at their default values (see Valdes 1982 for a detailed description). After this process, a visual inspection was carried out to eliminate catalogued objects that were clearly misclassified by FOCAS. In general, these objects were overlapping stars and/or galaxies forming a unique diffuse object mistaken for a galaxy. This type of contamination is estimated as $\sim 10\%$ of the whole catalog (see also de Carvalho, Ribeiro & Zepf 1994).

2.3. Magnitude Calibration and Limiting Magnitude

The calibration of the magnitude scale was done using CCD photometry from Postman & Lauer (1995) (hereafter PL) and Melnick & Quintana (1984) (hereafter MQ). PL obtained their data through actual photometric measurements of the cD galaxy (B-Johnson system) whereas the data from MQ is a compilation of measurements from the literature (in different passbands). Based on this, we decided to use the data from PL to do actual calibration, and to use the MQ data as a consistency test. Calibration was done by estimating the difference between the magnitude listed by PL and MQ and the instrumental total magnitude. FOCAS calculates the total luminosity by integrating the flux inside the “total area” of the object. This “total area” is in turn determined by fitting the concavities in x,y of the isotope shape and then adding rings around the object up to 2 times the detection area (called “grown area”). Consequently, the FOCAS instrumental magnitude beyond

the grown radius is constant. In this case PL provides measurements beyond the radius corresponding to the total area. For this reason, we have used the task “apphot” in IRAF to measure the instrumental magnitude within specific apertures. The internal apertures were not used due to saturation of the cD galaxy. The zero-point of the magnitude scale resulted in $K = 32.86 \pm 0.16$ (using data from PL) and $K = 32.92 \pm 0.18$ (using data from MQ). The comparison between the photometry results of PL, MQ and this work is shown in Figure 1 (top), with corresponding residuals (bottom).

The limiting magnitude of the catalog ($B_{lim} \sim 21$) was first estimated using the magnitude histogram of all detected objects not classified by FOCAS as “noise” objects, and was defined by the last bin prior to a significant counting decrease (Picard 1991). This magnitude limit estimate will be reanalysed in the next section.

2.4. The Final Galaxy Catalog

The photometric catalog described above was obtained by running FOCAS under its default classification rules by which the detected objects are assigned to 5 pre-defined “resolution” classes: n - noise, s - stars, sf - fuzzy stars, g - galaxy, and d - diffuse. A further class, “long”, is defined for those objects presenting flat and very elongated geometries. As discussed in detail by Valdes (1982), the uncertainties of such a classification are due, for one part, to the natural uncertainties in the partitioning of the image parameter space into astronomical classes and, for the other, to the rapid decrease of the classification probabilities at fainter magnitudes.

In order to circumvent these problems, which are indeed common to most automated astronomical image classifiers, we used a sample of 325 spectroscopically confirmed galaxies to provide an independent check to the FOCAS classifier performance. This sample was

obtained by compiling the following redshift catalogs: Bardelli et al. (1993), Mazure et al. (1997), Metcalfe et al. (1987), Melnick & Quintana (1984), Stein et al. (1996) and Teague et al. (1990). By cross-correlating it with our photometric catalog we produced a “matched” catalog consisting of 322 galaxies. For the remaining 3 galaxies, 2 were not included in the matched catalog because they were identified as multiple systems not split by FOCAS, and the other one could not be identified with any detected object. The statistics of FOCAS classification of these 322 objects is given in Table 1 (note that no galaxies were classified as “n”). As can be seen, the bright galaxies were correctly classified as “g” with a negligible contamination of the other classes. In contrast, faint galaxies are increasingly classified as “sf”. In view of these results, we conservatively decided to keep in the final catalog only objects classified as “g” and “sf”. This final galaxy catalog with 1421 galaxies is available from the AAS CDROM. We found, using the same methodology as Picard (1991), that the limiting magnitude of our catalog of galaxies is about the same as that of the initial photometric catalog (section 2.3), that is, $B_{lim} \sim 21$.

We have carried out a similar completeness analysis for the subset of galaxies with measured velocities. We found that it is only moderately complete in all magnitudes ranges (see Figure 2). Nevertheless, the completeness level per magnitude interval increases for galaxies systematically closer in projection to the central cD galaxy. For instance, a ~ 88 % cumulative completeness level up to the 17.5-18 mag bin is achieved for the galaxies within a 900 arcsec radius around the cD, whereas a ~ 95 % level up to the 18-18.5 mag bin is found using a 500 arcsec radius. These features are due to the inhomogeneities of the assembled velocity sample and will be taken into account in the dynamical analysis.

3. The Velocity Distribution

We have used the robust estimators discussed by Beers et al. (1990) to establish the membership of the final catalog of galaxies with measured velocities (322 galaxies) and to obtain the global kinematical parameters of A3558. A histogram of all measured velocities for the matched catalog (inset, Figure 3) was first used to eliminate the obvious foreground and background objects ($v < 9000 \text{ km s}^{-1}$ and $v > 18000 \text{ km s}^{-1}$). We then used the ROSTAT code (Beers et al. 1990, Beers et al. 1991) to compute the C_{BI} and S_{BI} estimators for the remaining velocities and recursively eliminated the galaxies that were 3 biweighted scales from C_{BI} (Teague et al. 1990), which converged to a membership criteria of $12000 \text{ km s}^{-1} < v < 18000 \text{ km s}^{-1}$. The final “velocity” catalog contains 282 possible member galaxies brighter than $B_{\text{lim}} \sim 21$. Its velocity histogram is shown in Figure 3. For comparison, the velocity histogram of galaxies within a 900 arcsec radius circle around the cD galaxy is shown on Figure 4. As argued in the previous section, this central subset ($R < 900 \text{ arcsec}$) is $\sim 88\%$ complete up to the 18 mag bin and may be taken as a representative sample of the core of A3558.

At this point we should note that the $1^\circ \times 1^\circ$ field covered by our photometry also includes, other than A3558 itself, the poor cluster SC1327-312 (RA = $13^h 30^m 04^s$, DEC = $-31^\circ 44' 49''$), first noted as a X-ray source by Breen et al. (1994). The velocity histogram of galaxies inside a circular region of 400 arcsec radius centered at the peak X-ray emission of SC1327-312 (Bardelli et al. 1996) is displayed in Figure 5. This sample, also defined for galaxies in the velocity range $12000 \text{ km s}^{-1} < v < 18000 \text{ km s}^{-1}$, contains 17 galaxies with measured velocities and is 82% complete down to 18 mag.

In Table 2 the global kinematical parameters of the 3 samples discussed above are presented. The columns are as follows: (1), sample; (2) and (3), C_{BI} and S_{BI} (in km s^{-1}) respectively, with their 90% confidence intervals; (4), numbers of galaxies used for the

estimate and (5), source reference. We will assume the redshift corresponding to the central ($R < 900$ arcsec) region as that representative for the cluster: $z = 0.0475 \pm 0.0003$.

We have performed several normality tests for the velocity distribution samples defined above using the ROSTAT code. The results indicate that the velocity distribution of A3558, using all 282 probable member galaxies, is consistent with normality under most of the statistical tests included in the ROSTAT routine (significance levels for the null hypothesis greater than 25%). The scaled tail index, $TI = 0.983$, indicates that the sample distribution is close to gaussian, whereas the asymmetry index, $AI = 0.971$, suggests that the distribution is skewed towards higher velocities (for a thorough discussion on these two indexes, see Bird & Beers 1993). Similarly, we find that the “core” $R < 900$ arcsec sample (Figure 4) is also approximately gaussian, with $TI = 0.942$ and $AI = 0.996$. The Dip test indicates that the probability of non-unimodality of the “core” sample is very large ($\sim 83\%$) and this result is in accordance with the presence of a bimodal core, as reported in detail in the next sections. The SC1327-312 sample (see Figure 5) displays an asymmetric distribution, $AI = -0.669$. We find a $TI = 0.768$ for this sample, which indicates that the tails are probably underpopulated, if the parent distribution is indeed gaussian, and the Dip test indicates that the probability of non-unimodality is reasonably high ($\sim 70\%$).

In order to discuss the importance of gaps in velocity space, we have followed the weighted gap analysis presented by Beers et al. (1992). A *single* gap is considered significant if its gaussian weighted value is greater than 2.25. Significant gaps found by sampling a gaussian distribution occur with a frequency less than 3%, independently of the sample size. The “total gap probability” (TGP) is another indicator of gap significance: it is the cumulative probability of finding a *number* N of individually significant gaps anywhere in the distribution. For instance, a low TGP indicates that, after resampling, all the N original gaps will very unlikely be found anywhere in the distribution, that is, the N gaps

will be collectively significant. We use the “stripe” density diagram to show the location of each significant gap (Beers et al. 1992). Each galaxy in velocity space is indicated by a unique vertical line, and significant gaps are indicated as arrows.

In the 282 galaxy sample velocity distribution (see upper diagram of Figure 3), we find that the probability of each individual gap is 0.03, except for one gap at ~ 13700 km s⁻¹, which is 0.002. Nevertheless, the “total gap probability” indicates that the probability that all these gaps occur anywhere in the distribution is greater than $\sim 40\%$. The “core” sample has several gaps. The position, size, weighted size and probability of each gap for this sample are: 13570 km s⁻¹ ($\Delta v = 79$ km s⁻¹, $z_* = 2.297$, $p = 0.03$), 15501 km s⁻¹ ($\Delta v = 172$ km s⁻¹, $z_* = 2.457$, $p = 0.03$), and 14505 km s⁻¹ ($\Delta v = 73$ km s⁻¹, $z_* = 2.470$, $p = 0.03$), 14640 km s⁻¹ ($\Delta v = 83$ km s⁻¹, $z_* = 2.580$, $p = 0.014$), 14425 km s⁻¹ ($\Delta v = 84$ km s⁻¹, $z_* = 2.658$, $p = 0.014$), and finally, 14763 km s⁻¹ ($\Delta v = 105$ km s⁻¹, $z_* = 2.803$, $p = 0.006$). The “total gap probability” is $\sim 21\%$ in this case: the occurrence of all these gaps anywhere in the distribution after resampling is relatively small. The SC1327-312 sample shows no significant gaps.

The presence of gaps indicates that the distribution probably has several “clumps” in the velocity space, but their overlapping makes separation impossible without positional information. A complete substructure analysis, using velocity/position data, is presented in the following section.

4. Substructure Analysis

4.1. Introduction

Clusters of galaxies can be morphologically arranged into an one-dimensional sequence (from irregular to regular) that suggests a direction of dynamical evolution (from young

to dynamically evolved systems). A virialized cluster is also expected to have a gaussian line-of-sight velocity profile, whereas a young system should present significant deviations from a gaussian profile in its velocity distribution. Although separate positional and velocity investigations can yield general clues about the global dynamical status of a cluster, only 3-dimensional (x, y, v) diagnostics can reduce the possibility of misinterpretation, since only combined correlations between position and velocity may define physical substructures, suggesting a non-equilibrium state of the cluster. Recent multi-fiber spectroscopy has allowed the construction of large scale redshift surveys (Zabludoff et al. 1993, Mazure et al. 1997) which, added to positional and photometric data, contributes to a reliable approach to the problem of substructure in clusters of galaxies (Bird 1994). Indeed, recent optical and X-ray observations (West 1994b and references therein) suggest that up to 75% of clusters show substructures in their morphologies.

The presence of substructures can also be analysed via global statistical tests which yield a substructure significance index for the data. These tests are especially useful for a general and direct comparative analysis of a large sample of clusters (see, e.g. Bird 1994), but they do not pinpoint the location, extension and dynamical nature of the substructures present in the data. For this reason, we shall adopt mapping techniques which are quite useful for this purpose.

4.2. Substructure Mapping and Dynamical Analysis

We use the Adaptive Kernel technique (AK, Silverman 1986) with a generalised Epanechnikov kernel in order to map the projected density of galaxies and also the local average velocities and the local velocity dispersion of galaxies (Biviano et al. 1996). Following Biviano et al. (1996), we have obtained significance maps for these quantities by taking the average of 1000 bootstraps of the original cluster and subtracting the

corresponding 3σ maps from this average. Structures that can “survive” this subtraction are statistically significant features at the 3σ significance level.

We have divided our field into three regions, namely: the *core region* defined by a square field of 1000 arcsec side centered on the cD galaxy, and encompassing most of the x-ray emission of the cluster. In this region the velocity sample is 89% complete down to $B \sim 19$; an *intermediate region* defined by a square field of 1800 arcsec side centered on the cD galaxy for which the velocity sample is 88% complete down to $B \sim 18$; and *the whole $1^\circ \times 1^\circ$ field*, for which the velocity sample is not complete at any limiting magnitude. All mappings have grids with 1 arcmin ($\simeq 0.05h_{75}^{-1} Mpc$) spacing. These AK maps are presented in Figs. 6-13, where in all figures the original cluster map is in the upper panel and the 3σ confidence map in the lower panel.

In order to analyse the substructures present in these figures, we use the Wavelet Transform technique (WT, Grossmann and Morlet 1987, Slezak et al. 1990) to generate the subcatalogs of galaxies for each substructure of interest (namely, the central substructures and the poor cluster SC1327-312). These subcatalogs were constructed by selecting galaxies inside a $2s$ radius around density peaks, where s is the wavelet scale which best characterizes the analysed structure (see Escalera et al. 1994 and Slezak et al. 1990 for details).

The core region (Figs. 10-12) features a significant bimodal structure (denoted by A and B in all maps). This central region is thoroughly analysed in the following subsections. The apparent central bimodal core is also found in the intermediate region map (Figure 6), where several significant substructures (at 3σ significance level) are also present. Statistically significant average velocity and velocity dispersion structures can also be noted (Figures 7 and 8, respectively). The whole field around A3558 is clearly marked with several substructures (Figure 9). The poor cluster SC1327-312 towards the southeast, known *a priori* to be partially represented on our field, is also clearly detected. Unfortunately the

incompleteness of the velocity catalog for the whole region does not allow us to assess the reality of most these substructures. However, as we argue below, their abundance and projected distribution suggests that the infall region of A3558 (> 1 Mpc) may be composed of several groups of galaxies in the process of merging.

Indeed, we qualitatively note a “preferential alignment” at the $\sim 45^\circ$ position angle of a diverse set of features in this cluster, ranging from small to large scales. An application of the Lee-statistics (Fitchett 1988) to this cluster also indicates that the $\sim 45^\circ$ direction has a greater probability of bimodality. This alignment coincides with (a) the major axis PA of the dominant galaxy, (b) the major axis PA of the isocontours of the central core (using AK/WT maps as well as a X-ray countour map), (c) a marginal velocity gradient direction across the central bimodal substructures, and (d) the direction of alignment of major subclumps, namely the bimodal core and SC1327-312. This alignment seems to persist even beyond the analysed field. A qualitative inspection of an isopleth map of a $\sim 32^\circ \times 32^\circ$ region around A3558 (see Figure 2 of Raychaudhury et al.1991), also indicates an alignment of all major clusters in the Hydra-Centaurus region spanning from position angles of $\sim 40^\circ$ to $\sim 60^\circ$. Considering the physical dimensions involved, it is quite surprising that the average alignment of major clusters in the Shapley Concentration is consistent with the direction of alignment of several substructures within A3558 and with the major axis position angle of its dominant galaxy. We find that these small to large scale “coincidental” associations (namely, cD major axis match to the general clustering alignment) can be taken as an observational evidence of an anisotropic merger scenario as for instance the one proposed by West (1994a).

4.2.1. *The complexity of the central core of A3558*

Figure 10 (upper panel) presents the projected density contour map of the very central core of A3558. It shows a clear bimodal structure which is very prominent on the 3σ confidence map, as can be seen in the lower panel of this figure. The two central clumps are labeled “A” (RA = $13^h27^m49^s$, DEC = $-31^\circ28'59''$) and “B” (RA = $13^h28^m13^s$, DEC = $-31^\circ33'10''$) in Table 3. The average velocities of these central substructures are also significantly distinct, as can be seen in Figure 11 and also by an inspection of the C_{BI} values displayed in Table 3 (the difference of their average velocities are out their 90central location). The isodispersion map (Figure 12) indicates that the average velocity dispersion of substructure A differs from that of the central region, although not very significantly. This is also in accordance with the S_{BI} values listed in Table 3.

Figure 13 displays the projected density contour map of the faint galaxy subsample of the core region ($19 < B < 21$). The distribution of faint galaxies is much smoother than that of the brighter galaxies, having peak densities which attain no more than half of those of the bright subsample. Both substructures A and B are still present in this map, but much less prominently. There are also hints of new significant clumps which are mapped only by faint galaxies. Unfortunately, this faint central subsample contains only 5 galaxies with measured velocities (all of them in the range $12000 < v < 18000 \text{ km s}^{-1}$) precluding a more detailed analysis about the possible existence of background clusters.

The above discussion stresses the apparent complexity of the central core of A3558. This is to be contrasted to the featureless X-ray emission, Figure 14, which is centered on the cD galaxy with a smooth extension towards the location of substructure B (see also the detailed study by Bardelli et al. 1996). This suggests that the gas is driven by a smooth gravitational potential which does not seem to be mapped by the bright galaxy component of the cluster. We are thus led to conjecture that the projected core of A3558 is made of 3

dynamically distinct structures: the main virialized core of the cluster, which is traced by the X-ray gas and maybe also by the faint galaxy component; and the galaxy clumps A and B, described before.

4.2.2. Solving the cD offset

To support the picture described above, we have verified that the velocity histogram of substructure A is apparently bimodal (see Figure 15). Indeed, as noticed previously, the asymmetry index of the velocity distribution of the $R < 900$ arcsec sample is 0.996. This suggests that there is a high velocity population excess, and this may be partially due to substructure A. The statistics of substructure A velocity distribution indicates a scaled tail index at 0.886 and no significant gaps where found. We notice that one of the two peaks of the velocity distribution of substructure A is centered very nearly at the velocity of the cD. The Dip test applied to this sample indicates that the probability of non-unimodality is ~ 30 %. Both peaks also seems to have a reasonably narrow dispersion, suggesting that clump A galaxies may be separated into two subsamples: galaxies with $v < 14750$ km s⁻¹ belong to the core sample defined above, and galaxies with $v > 14750$ km s⁻¹ form the actual background group A. This group is denoted in Table 3 as A'.

Figure 16 shows the isodensity map which results from removing the A' galaxies from the core region (this new sample is denoted in Table 3 as “core - A'”). There is no sign of any clumping at the location where substructure A was previously detected. The average velocity of this core sample is almost exactly the same as that of the cD galaxy (14030 ± 42 km s⁻¹), that is, the velocity offset of the cD is contained within the 90 % interval on central location in velocity space and is no longer significant (see the confidence limits on Table 3).

4.2.3. *The β -problem revisited*

The velocity dispersion for the new core sample discussed above is much smaller than the value generally quoted for A3558 (see Table 3) which, for instance, led *ardelli et al.* (1996) to postulate a “strong β -problem” for A3558. Assuming the new value given in Table 3, we find $\beta_{spec} = 1.13$ (0.93,1.31), to be compared with $\beta_{fit} = 0.611$ estimated by *Bardelli et al.* (1996) from fitting the X-ray brightness to an isothermal model. A β -problem still remains, but can no longer be considered “extreme” (the β_{spec} value found by *Bardelli et al.* 1996 for A3558 is 1.79).

Nevertheless, the above results may be improved by further removing substructure B galaxies from the core sample. This removal may be justified if we interpret the X-ray extension towards B as due to the gas response to a local fluctuation of the gravitational potential due to B. This interpretation is corroborated by the WT analysis of the X-ray emission of A3558 given by *Slezak et al.* (1994), which shows evidence for a X-ray counterpart for substructure B. Since the dynamical time of collision for the gas is much shorter than for the galaxies, we can assume that the infall of subclump B galaxies is still a recent event and has not strongly disturbed the dynamics of the core. The kinematical parameters for the sample obtained by removing substructure B from the core defined before are given in Table 3. Notice that the difference between the cD velocity and the mean velocity of the core is further reduced for this sample. We now find $\beta_{spec} = 0.89$ (0.66,1.22) which is much closer to β_{fit} than the previous calculated value. Moreover, if we take into account the more reliable ASCA temperatures for A3558 given by *Markevitch, Sarazin, & Henriksen* (1996), we will find that $\beta_{spec} = 0.70$ (0.55,0.85), a value which coincides almost exactly with $\beta_{fit} = 0.611$ estimated by *Bardelli et al.* Notice that using the global core velocity dispersion (i.e, without removing substructure B), together with ASCA temperatures, gives $\beta_{spec} = 1.09$ (0.89,1.29), to be compared to the value quoted

by Bardelli et al. of 1.79, using the more uncertain ROSAT temperatures (Markevitch, Sarazin, & Henriksen 1996).

According to Bahcall & Lubin (1993), a solution for the β -problem arises naturally if an empiric spatial $r^{-2.4}$ law, fitted for the cluster outer region ($> 1.5Mpc$), is used instead of a King law. Since we found that the β -discrepancy for A3558 could also be naturally diminished by using a better estimation of the velocity dispersion, we analysed in detail the density profile to check the above hypothesis. We compared the projected density profile of galaxies in the central region to the X-ray brightness profile. This profile, given by Bardelli et al. (1996), is an elliptical King law fit to the overall cluster emission. By taking the axial ratio and position angle derived from their fit, we find that the projected central density profile of galaxies could also be very well fitted by a King law. This is in agreement with the hypothesis that our selected sample represents the relaxed core component, with the galaxies in equilibrium with the emitting gas. However, the galaxy sample selected from the whole region of our plate could only be fitted by the sum of 2 King profiles, one of which clearly represents the core component whereas the other, with have a very large core radius, probably represents a background component. At the wings of the projected galaxy distribution, the resulting combined profile tends towards a $\sim r^{-1.5}$, very similar to the one proposed by Bahcall & Lubin.

4.3. Mass Estimates

We derive mass estimates for A3558 under the hypothesis that (1) the system is self-gravitating (we refer to this mass estimate as $M_{selfgrav}$; Heisler, Tremaine & Bahcall 1985) and (2) the galaxies orbit around a common central potential (M_{sat} ; Bahcall & Tremaine 1981). The mass estimates are calculated for increasing circular regions centered on the cD, after removing galaxies belonging to substructure A'. We have also calculated the

mass of the poor cluster SC1327-312. The resulting values are listed in Table 4. Columns are: (1) label; (2) aperture radius in Mpc centered on the cD; (3) number of galaxies defining the region; (4) and (5) C_{BI} and S_{BI} in km s^{-1} , respectively together with their 90% confidence limits; (6) mass in units of $10^{14} h_{75}^{-1} M_{\odot}$, according to Heisler, Tremaine & Bahcall 1985 and estimated error; (7) mass in units of $10^{14} h_{75}^{-1} M_{\odot}$, according to Bahcall & Tremaine 1981 and estimated error; and (8) M_{sat}/L ratio in units of $10^3 M_{\odot}/L_{\odot}$, the total luminosity being computed down to $B = 19$.

Figure 17 shows the comparison of our results to others found in the literature. Our results, based on the self-gravitating hypothesis, are compatible (although systematically higher) with previous dynamical estimates found by Biviano et al. (1993), Metcalfe et al. (1987) and Metcalfe et al. (1994), based on different samples. Although systematically higher by a factor ~ 2 , our results based on the “satellite” hypothesis provide lower values for the mass estimates, which are more compatible with the mass estimates provided by Bardelli et al. (1996), based on X-ray data. This is consistent with the fact that most of the cluster mass is not bound to the visible galaxies. The discrepancy between our mass estimates compared to the X-ray total mass estimates may be partially explained by the presence of substructures which were not well taken in account in our calculations (Bird 1994). Indeed, only substructure A' could be reasonably isolated in velocity space. We note that, within errors, the M/L ratio is approximately constant with radius distance, averaging to about $250 M_{\odot}/L_{\odot}$ (the poor cluster SC1327-312 also has a M/L ratio consistent with that of A3558). This suggests that galaxies follow the same distribution as the total cluster mass, as already noted by Bardelli et al. (1996).

5. Discussion

In this paper, we examine the cluster of galaxies A3558, focusing on substructure analysis, using position and velocity data. We find that a simple analysis of the velocity distribution is not sufficient to resolve the cluster into multiple components. Only a 3-D analysis can establish the nature of these subsystems.

The AK isodensity, isovelocity and isodispersion maps and the WT analysis all indicate that the region defining A3558 is actually composed of a collection of several groups of galaxies, suggesting that A3558 is a dynamically complex, young cluster of galaxies. This conclusion is consistent with recent results (Bardelli et al. 1996, Markevitch, Sarazin, & Henriksen 1996) using independent (namely, X-ray) data.

We also find a “preferential alignment” at the $\sim 45^\circ$ position angle of a diverse set of features in this cluster, ranging from small to large scales. In addition to this result, the number statistics of the bright X-ray clusters in the Hydra-Centaurus region also demonstrates the presence of a linear feature which is not a chance aggregation of clusters (Raychaudhury et al. 1991). As Shapley himself noted, the supercluster which bears his name is notable due to “its great linear dimension, the numerous population, and distinctly elongated form” (Shapley 1930). Although standing only as a qualitative analysis, our results can be taken as observational support of an anisotropic merger scenario (West 1994a; see also Rhee, van Haarlem & Katgert 1992, Plionis 1994). Other observational support for such scenario comes from an analysis of correlations between the spatial distribution of substructures and the surrounding matter found in a sample of 7 X-ray clusters with at least three major subclumps (West et al. 1995). Other similar examples of substructure/large scale distribution alignments are: the Coma cluster (West et al. 1995), A426 (Schwarz et al. 1992) and AWM7 (Stern et al. 1995).

Our analysis of the cluster core clearly indicates that the cD velocity offset is no longer

observed. This is interesting because it is generally supposed that dominant cD galaxies in clusters are formed out of debris of disrupted galaxies orbiting near the center-of-mass (CM) of the clusters and/or by accretion of intracluster gas from a cooling flow, so their velocities should reflect that of the cluster CM. Also, this result is compatible with the analysis of Gebhardt & Beers 1991, where the authors suggested that a large fraction of clusters in their data sample that presented significant cD offsets could be examples of clusters with real substructure. Our results are also compatible with the study of Bird 1994 on the correlation between the cD offset and the degree of substructuring.

Concerning the β -problem, although the incompleteness in velocity data of our catalog at regions greater than 1.5 Mpc forbids a direct check of Bahcall & Lubin (1993) hypothesis, a background component could be responsible, at least partially, for the observed $r^{-2.4}$ law. However, only a complete velocity sample for the outer cluster region can establish whether the $r^{-2.4}$ law represents a real trend in cluster density profiles or not. Such analysis would be extremely important for our understanding of cluster formation.

It is interesting to note that our results imply that: (1) the intracluster gas and the galaxies are in approximate thermodynamic equilibrium ($\beta_{spec} = \beta_{fit}$); (2) the intracluster gas is more spread in phase-space than the galaxies ($\beta_{spec} < 1$). This implies no β -discrepancy for A3558, but a mechanism to explain why $\beta_{spec} < 1$ is necessary. An early satellite merger with A3558 is suggestive, since the ellipsoidal external x-ray isophotes of the cluster could be interpreted as a merger signature. Finally, our results indicate that a superestimation of the velocity dispersion due to substructure contamination is clearly an important factor contributing to the arisal of the β -discrepancy in clusters.

We thank Timothy Beers for providing the ROSTAT code and the first version of the Adaptive Kernel program. His valuable referee comments were also very helpfull for improving the final version of this manuscript and we thank him for that. We also thank

Andrea Biviano for discussions about the bootstrapping techniques used in this work. One of us (C.C.D.) acknowledges a fellowship from CAPES. This work has been partly supported by a CNPq-CNRS grant.

REFERENCES

- Abell, G. O., Corwin Jr., H. G., & Olowin, R. P., *ApJS*, 1989, 70, 1.
- Ashman K. M., Bird, C. & Zepf, S. E., *AJ*, 1995, 108, 2348.
- Bahcall, N. A. & Lubin, L. M., *ApJ*, 1994, 426, 513 .
- Bahcall, J. N. & Tremaine, S., *ApJ*, 1981, 244, 805.
- Bardelli, S., Zucca, E., Vettolani, G., Zamorani, G., Scaramella, R., Collins, C. A.,
MacGillivray, H. T., *MNRAS*, 1994, 267, 665.
- Bardelli, S., Zucca, E., Malizia, A., Zamorani, G., Scaramella, R. & Vettolani G., *A & A*,
1996, 305, 435.
- Beers, T. C., Flynn, K. & Gebhardt, C., *ApJ*, 1990, 100, 32.
- Beers, T. C., Forman, W., Huchra, J. P., Jones, C., & Gebhardt, K., *AJ*, 1991, 102, 1581.
- Beers, T. C., Gebhardt, K., Huchra, J. P., Forman, W., Jones, C. and Bothun, G., *ApJ*,
1992, 400, 410.
- Bird, C.M. & Beers, T., *AJ*, 1993, 105, 1596.
- Bird, C. M., PhD Thesis, University of Minnesota, 1994.
- Breen, J., Raychaudhury, S., Forman, W., Jones, C., *ApJ*, 1994, 424, 59
- Biviano, A., Girardi, M., Giuricin, G., Mardirossian, F. & Mezzetti, M., *ApJ*, 1993, L13.
- Biviano, A., Durret, F., Gerbal, D., Le Fevre, O., Lobo, C., Mazure, A., Slezak, E.. *A & A*,
1996, 311, 95.

Dantas, C. C. de Carvalho, R. R. & Capelato, H. V. in Proceedings of the XXIXth Rencontre de Moriond, Clusters of Galaxies, ed. F. Durret, A. Mazure & J. Trân Than Vân, 1994, p.385.

Dantas, C. C., MS thesis, INPE/MCT, Brazil, 1996.

de Carvalho, R. R., Ribeiro, A. L. B. & Zepf, S., ApJS, 1994, 93, 47.

Dressler, A. & Schectman, S., AJ, 1988, 95, 284.

Escalera, E., Biviano, A., Giardi, M., Giuricin, G., Mardirossian, F., Mazure, A., Mezzetti, M., ApJ, 1994, 423, 539.

Fitchett, M. J., MNRAS, 1988, 230, 161.

Gebhardt, K., & Beers, T. C., 1991, ApJ 383, 72.

Gerbai, D., Durret, F., Lachièze-Rey, M., 1994, A & A, 288, 746.

Geller, M. J. & Beers, T. C., PASP, 1982, 94, 421.

Gorenstein, P., Fabricant, D., Topka, K., Harnden Jr, F. R., Tucker, W. H., 1978, ApJ, 224, 718

Grossmann, A. & Morlet, J., Mathematics and Physics, Lectures on Recent Results, ed. L. Streit, World Scientific, 1987.

Heisler, J., Tremaine, S. & Bahcall, J. N., ApJ, 1985, 298, 8.

Jones, C. & Forman, W., 1984, ApJ, 276, 38.

Katz, N & White, S. D. M., ApJ, 1993, 412, 455.

Kriessler, J. R. & Beers, T. C., AJ, 1997, in press.

Lasker, B. M. et al., *AJ*99, 1990, 99, 2019.

Markevitch, M. L., Sarazin, C. L. & Henriksen, M. J., 1996, *ApJ* submitted.

Mazure et al. 1997, in preparation.

Melnick, J. & Quintana, H., *A&A*, 1981, 44, 67.

Melnick, J. & Quintana, H., *AJ*, 1984, 89, 1288.

Metcalfe, N., Godwin, J. G., & Spenser, S. D., *MNRAS*, 1987, 225, 581.

Metcalfe, N., Godwin, J. G., & Peach, J. V., *MNRAS*, 1994, 267, 431.

Picard, A. 1991, PhD Thesis, California Institute of Technology.

Plionis, M., *ApJS*, 1994, 95, 401.

Postman, M. & Lauer, T. R., *ApJ*, 1995 440, 28.

Raychaudhury, S., Fabian, A. C., Edge, A. C., Jones, C., Forman, W., *MNRAS*, 1991, 248,
101.

Rhee, G., van Haarlem, M., & Katgert, P., *AJ*, 1992, 103, 1721.

Richstone, D., Loeb, A. & Turner, E. L.. *ApJ*, 1992, 393, 477.

Schwarz, R. A., Edge, A. C., Voges, W., Bohringer, H., Ebeling, H., & Briel, U. G., *å*, 1992,
256, L11.

Shapley, H., *Bull. Harvard Obs.*, 1930, 874, 9.

Silverman, B. W., *Density Estimation for Statistics and Data Analysis*, Chapman & Hall,
1986.

Slezak, E., Bijaoui, A., Mars, A., *A&A*, 1990, 227, 301.

- Slezak, E., Durret, F. and Gerbal, D., *AJ*, 1994, 108, 1996.
- Stein, P., *A&AS*, 1996, 116, 203.
- Stern, C., Jones, C., Hughes, J. & Forman, W., *ApJS*, 1995, submitted.
- Teague, P. F., Carter, D. & Gray, P. M., *ApJS*, 1990, 72, 715.
- West, M. J. & Bothun, G. D., *ApJ*, 1990, 350, 36.
- West, M. J., *MNRAS*, 1994, 268, 79.
- West, M. J., in Proceedings of the XXIXth Rencontre de Moriond, Clusters of Galaxies, ed. F. Durret, A. Mazure & J. Trân Thanh Vân, 1994.
- West, M. J., Jones, C., & Forman, W., *ApJ*, 1995, 451, L5.
- Whitmore, B. C., em “Clusters of Galaxies - Space Telescope Science Institute Symposium Series”, number 4, page 139, 1990.
- Valdes, F., Instrumentation in Astronomy IV, S.P.I.E. Proceedings, Vol. 331, 1982.
- Zabludoff, A., Geller, M., Huchra, J. & Ramella, M., *AJ*, 1993, 106, 1301.
- Zucca. E., Zamorani, G., Scaramella, R., Vettolani, G. 1993, *ApJ*, 407, 470.

Fig. 1.— Comparison between the photometry results of PL, MQ and this work, with corresponding residuals (where ΔB is the difference between ours and PL, MQ results).

Fig. 2.— Magnitude histograms of the photometric catalog (solid line), including all detected objects classified as “g” and “sf”, and the velocity matched catalog with 322 galaxies (dotted line). The magnitude limit based on Picard’s methodology (1991) is marked with an arrow.

Fig. 3.— *Inset:* Velocity histogram of the matched catalog with 322 objects. *Figure:* Velocity histogram for the final 3 S_{BI} -clipped matched catalog with 282 objects. *Upper diagram:* “Stripe” density plot for the velocity distribution; gaps are indicated as arrows.

Fig. 4.— Velocity histogram for the $R < 900$ arcsec sample. *Upper diagram:* “Stripe” density plot for the velocity distribution; gaps are indicated as arrows.

Fig. 5.— Velocity histogram for the SC1327-312 sample. *Upper diagram:* “Stripe” density plot for the velocity distribution; gaps are indicated as arrows.

Fig. 6.— Isodensity contour map using the Adaptive Kernel technique (top) and its -3σ significance level map (bottom) for the *intermediate region* centered at the cD galaxy (represented by a solid square). North is up and east to the left; both axis have ticks equally spaced by 300 arcsecs. *Top:* contoured from 0 to 2×10^{-4} gal deg $^{-2}$, in intervals of 2×10^{-5} . *Bottom:* contoured from 0 to 9.6×10^{-5} gal deg $^{-2}$, in intervals of 6×10^{-6} .

Fig. 7.— Same as Figure 6 for the local average velocity contour map. *Top:* contoured from 13100 to 15600 km s $^{-1}$, in intervals of 200 km s $^{-1}$. *Bottom:* contoured from 10000 to 14200 km s $^{-1}$, in intervals of 600 km s $^{-1}$.

Fig. 8.— Same as Figure 6 for the local velocity dispersion contour map. *Top:* contoured from 0 to 1800 km s $^{-1}$, in intervals of 200 km s $^{-1}$. *Bottom:* contoured from 0 to 1000 km

s^{-1} , in intervals of 200 km s^{-1} .

Fig. 9.— Isodensity contour map using the Adaptive Kernel technique (top) and its -3σ significance level map (bottom) for the whole field of A3558 ($B_{lim} = 19$). The position of the cD galaxy is represented by a solid square. North is up and east to the left; both axis have ticks equally spaced by 500 arcsecs. *Top*: contoured from 0 to $4 \times 10^{-4} \text{ gal deg}^{-2}$, in intervals of 2×10^{-5} . *Bottom*: contoured from 0 to $2.6 \times 10^{-4} \text{ gal deg}^{-2}$, in intervals of 1.3×10^{-5} .

Fig. 10.— Isodensity contour map using the Adaptive Kernel technique (top) and its -3σ significance level map (bottom) for the central *core region* centered at the cD galaxy (represented by a solid square). North is up and east to the left; both axis have ticks equally spaced by 200 arcsecs. *Top*: contoured from 0 to $4 \times 10^{-4} \text{ gal deg}^{-2}$, in intervals of 2×10^{-5} . *Bottom*: contoured from 0 to $1.4 \times 10^{-4} \text{ gal deg}^{-2}$, in intervals of 2×10^{-5} .

Fig. 11.— Same as Figure 10 for the local average velocity contour map. *Top*: contoured from 13100 to 15700 km s^{-1} , in intervals of 200 km s^{-1} . *Bottom*: contoured from 10000 to 14500 km s^{-1} , in intervals of 500 km s^{-1} .

Fig. 12.— Same as Figure 10 for the local velocity dispersion contour map. *Top*: contoured from 100 to 1300 km s^{-1} , in intervals of 200 km s^{-1} . *Bottom*: contoured from 0 to 675 km s^{-1} , in intervals of 75 km s^{-1} .

Fig. 13.— As in Figure 10, we plot the isodensity contour map for the *central core* sample of faint galaxies $19 < B < 21$. *Top*: contoured from 0 to $3.2 \times 10^{-4} \text{ gal deg}^{-2}$, in intervals of 2×10^{-5} . *Bottom*: contoured from 0 to 1.7×10^{-4} galaxies per square degree, in intervals of 1×10^{-5} .

Fig. 14.— X-ray contour map of the central *core region* (*top*) and the whole field (*bottom*).

Both maps are centered in the cD galaxy (solid square) and may be directly compared to the isodensity maps of Figures 10 and 9 respectively.

Fig. 15.— Velocity histogram for the A sample. *Upper diagram*: “Stripe” density plot for the velocity distribution.

Fig. 16.— Isodensity contour map for the central *core region* with substructure A removed as described in the text. Contour levels are the same as in Fig 10.

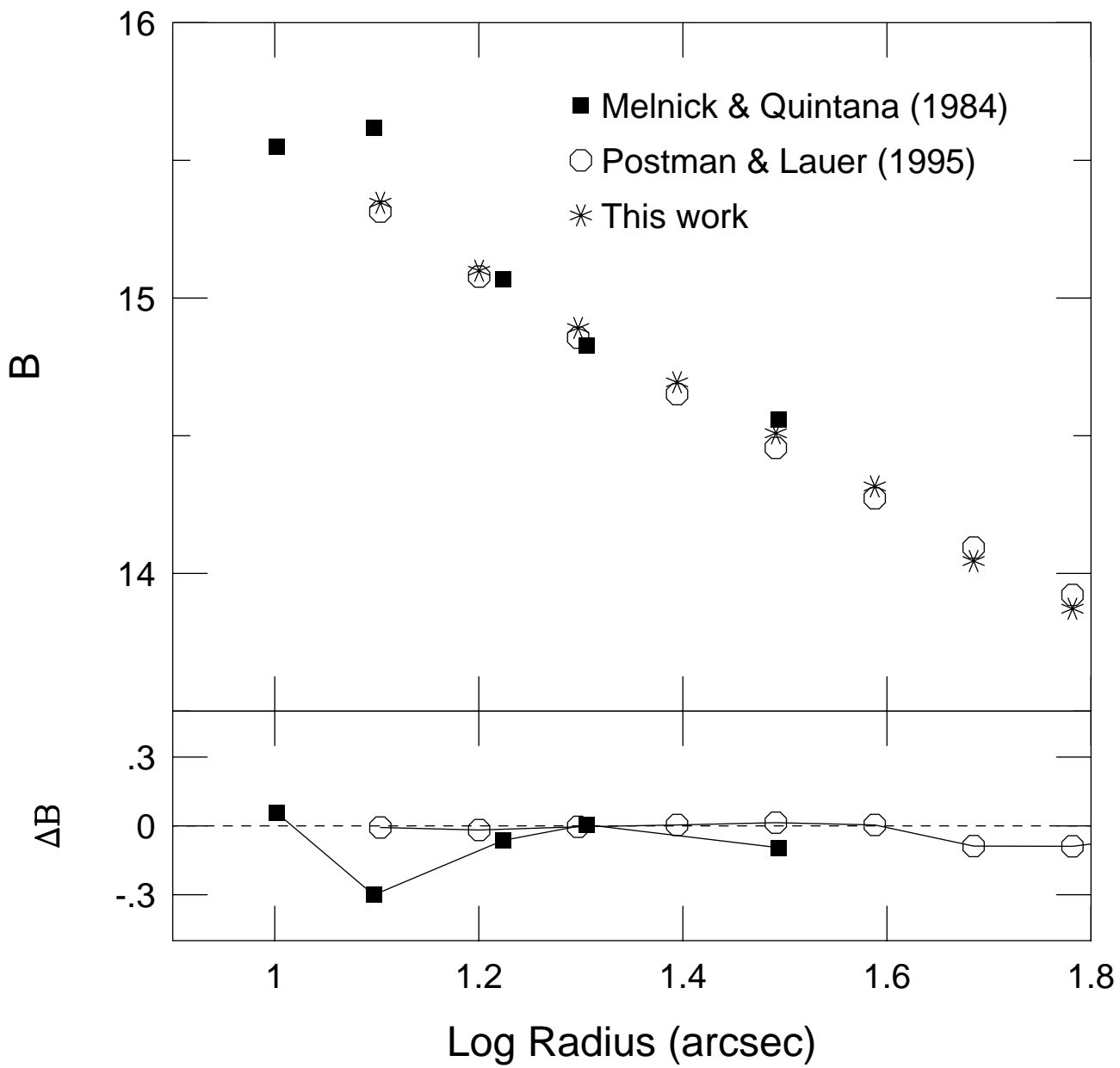
Fig. 17.— Mass estimates (in units of $10^{14} h_{75}^{-1} M_{\odot}$) within given aperture radii (in Mpc) centered around the cD galaxy, accordingly to several authors.

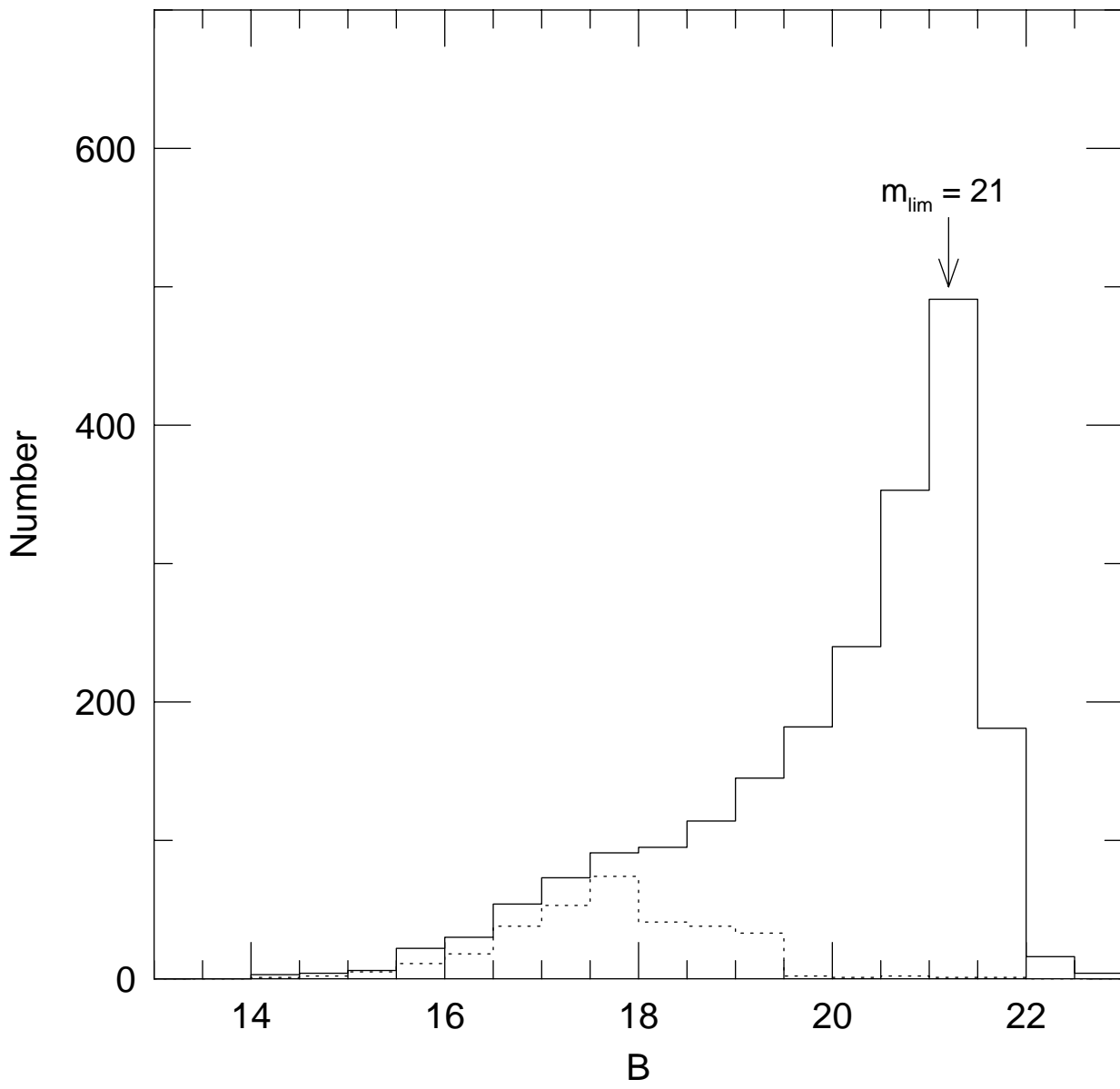
Table 1:

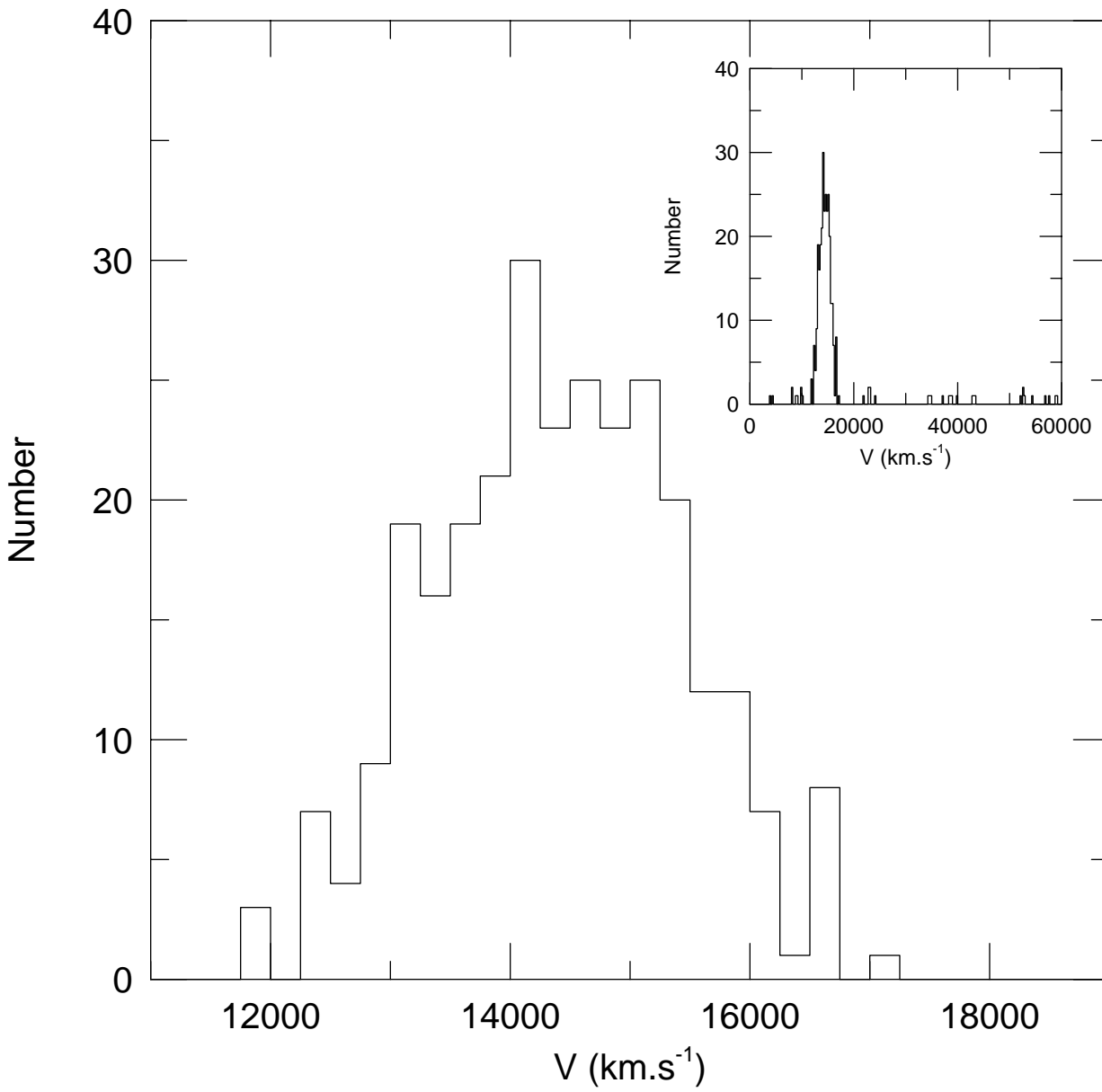
Table 2:

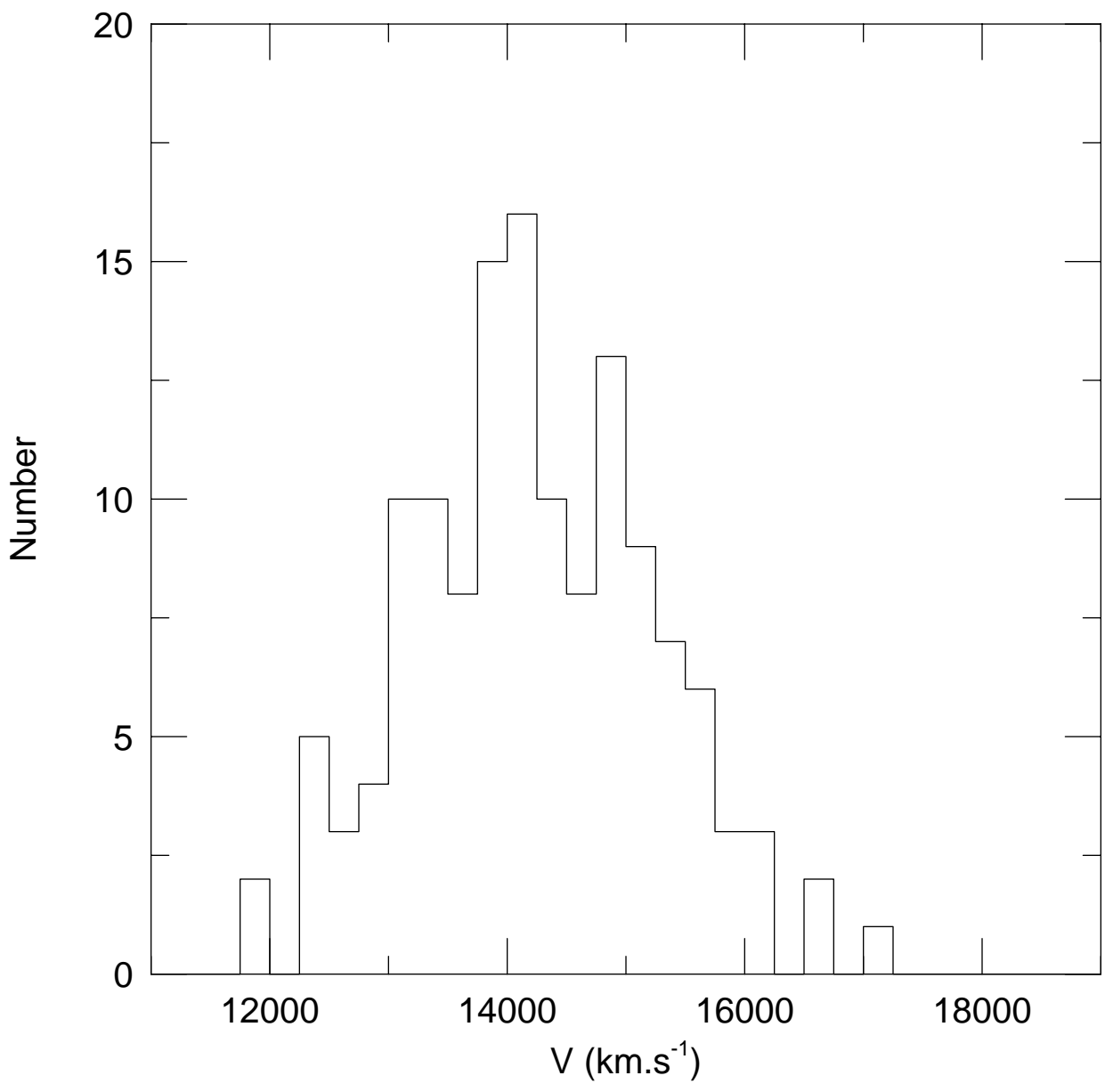
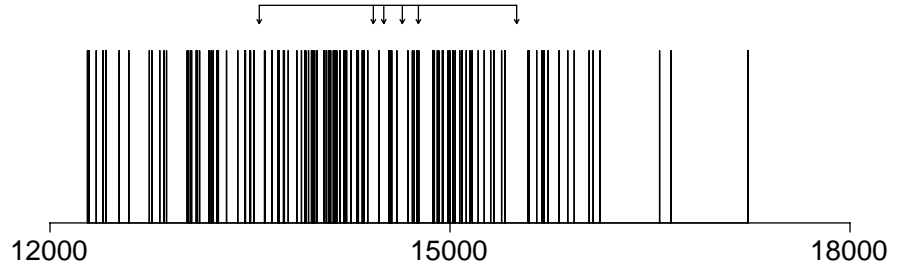
Table 3:

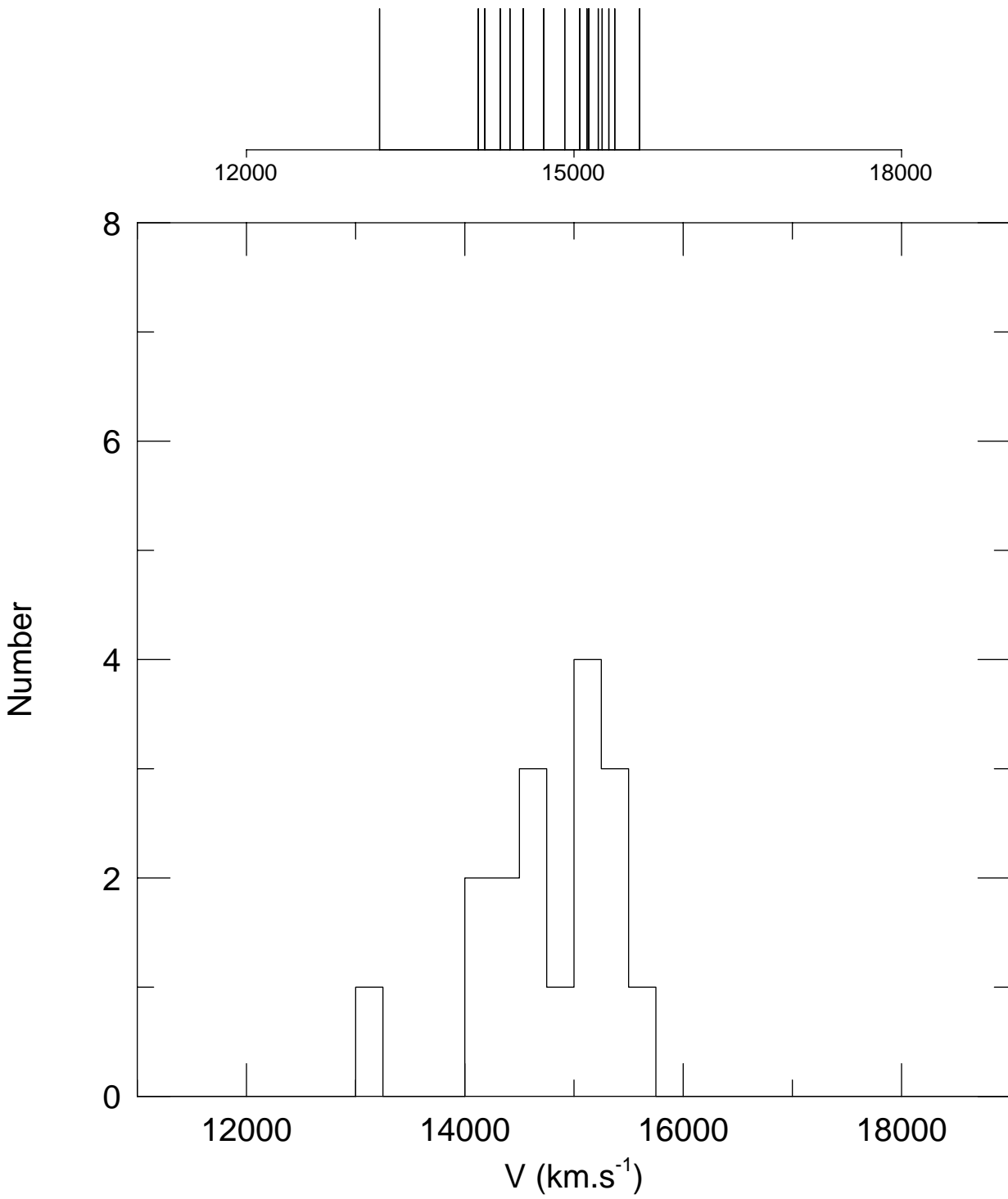
Table 4:



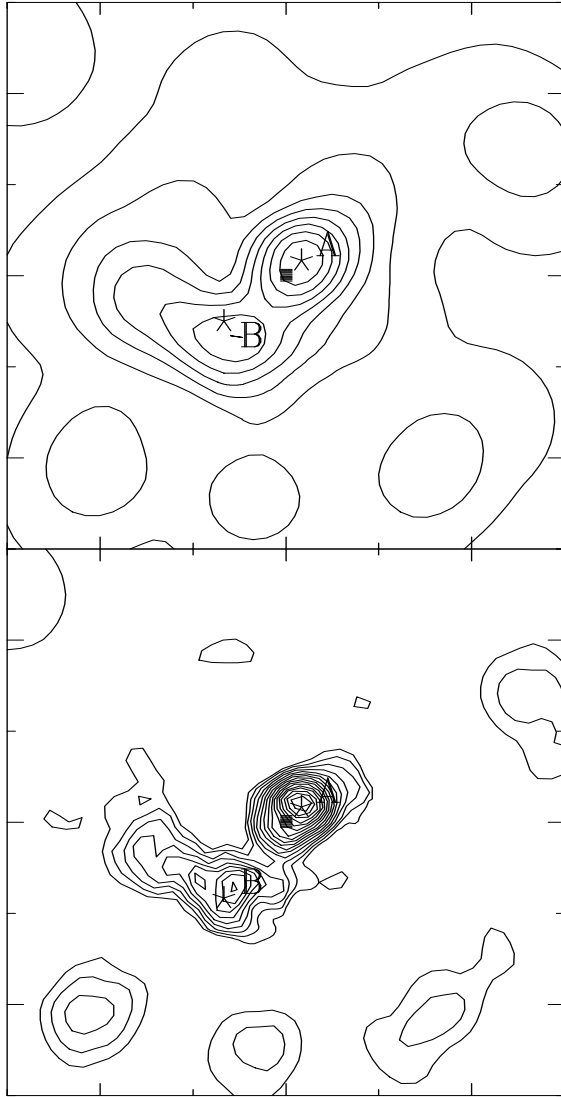




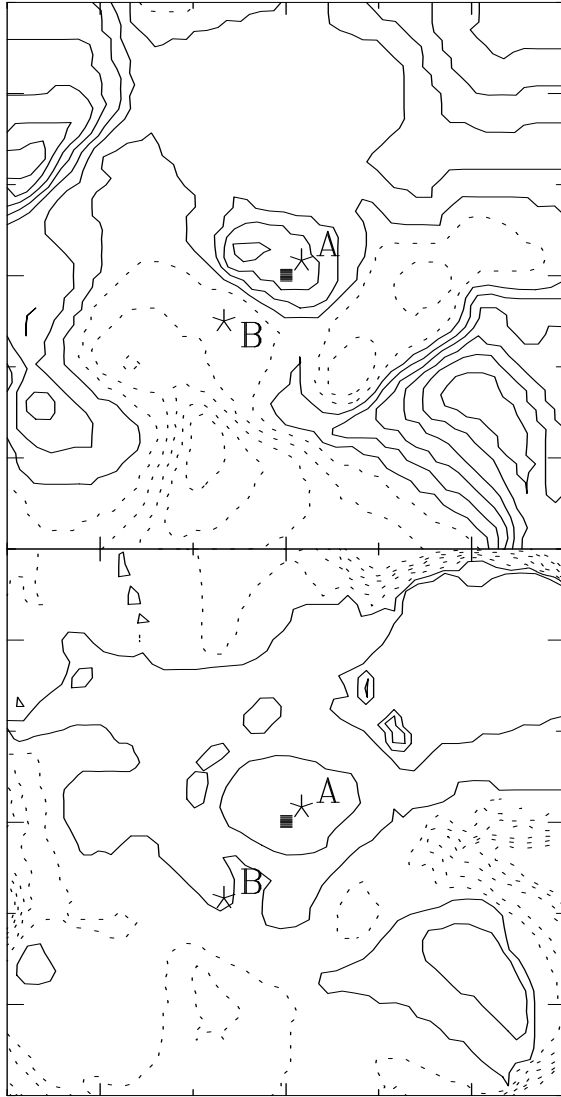




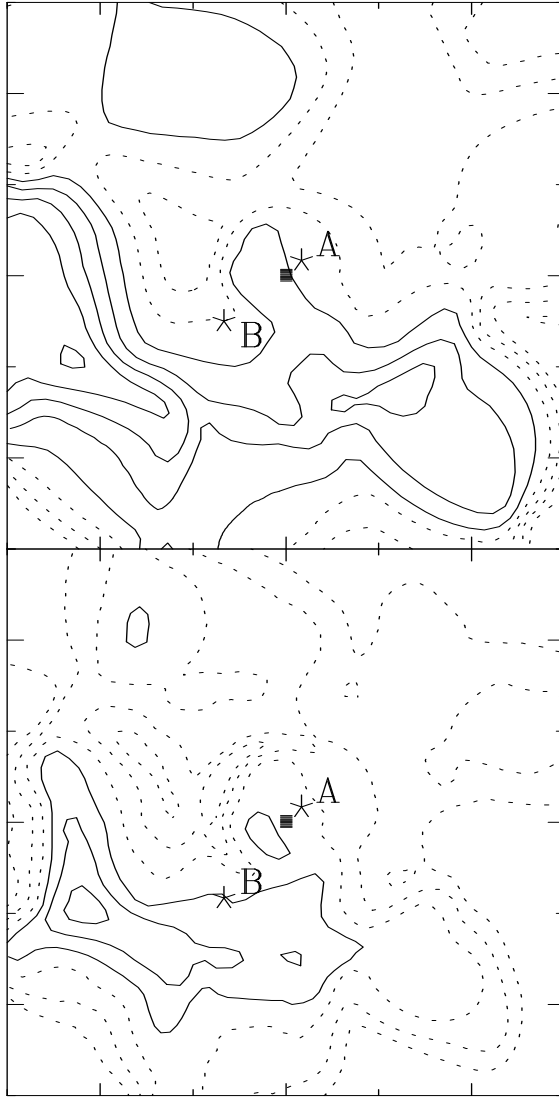
0.5 h_{75}^{-1} Mpc



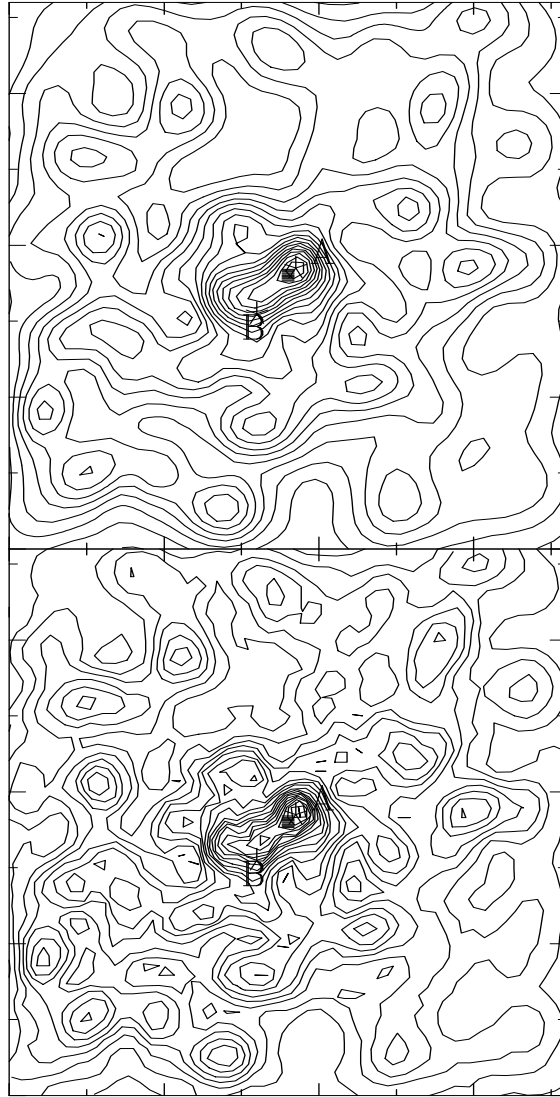
0.5 h_{75}^{-1} Mpc



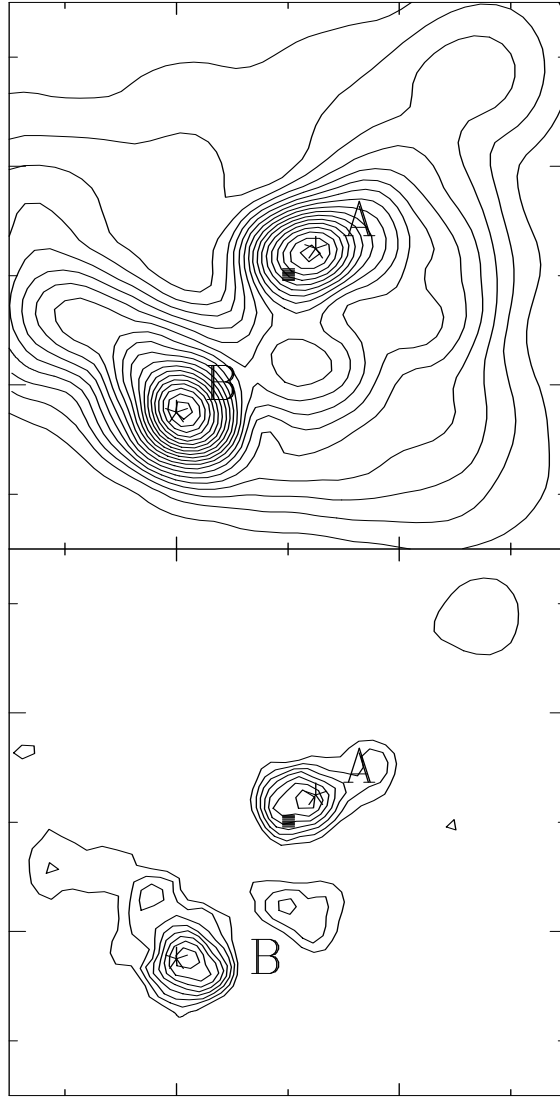
0.5 h_{75}^{-1} Mpc



0.5 h_{75}^{-1} Mpc

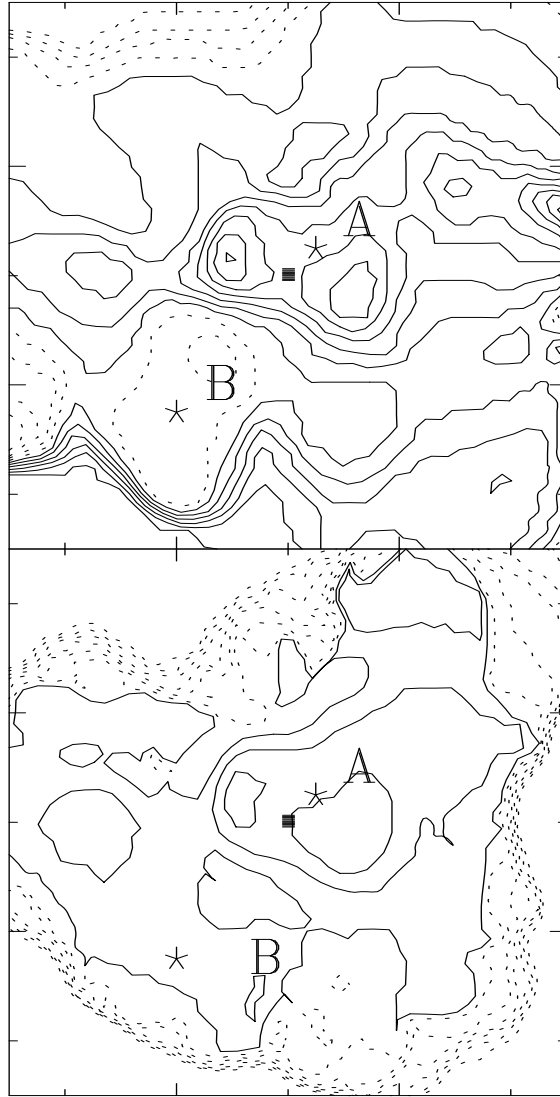


0.1 h_{75}^{-1} Mpc



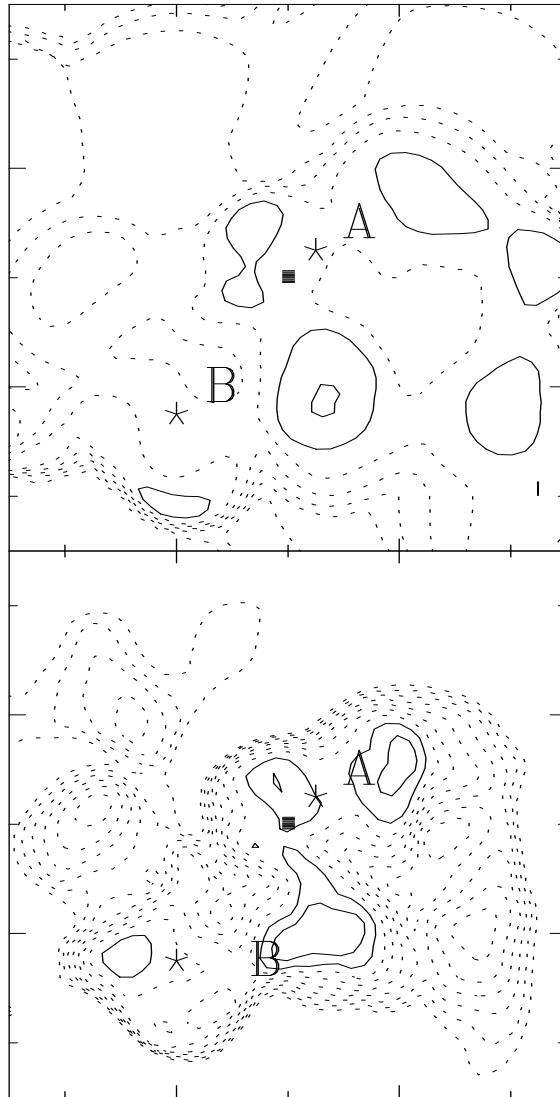


$0.1 h_{75}^{-1} \text{ Mpc}$



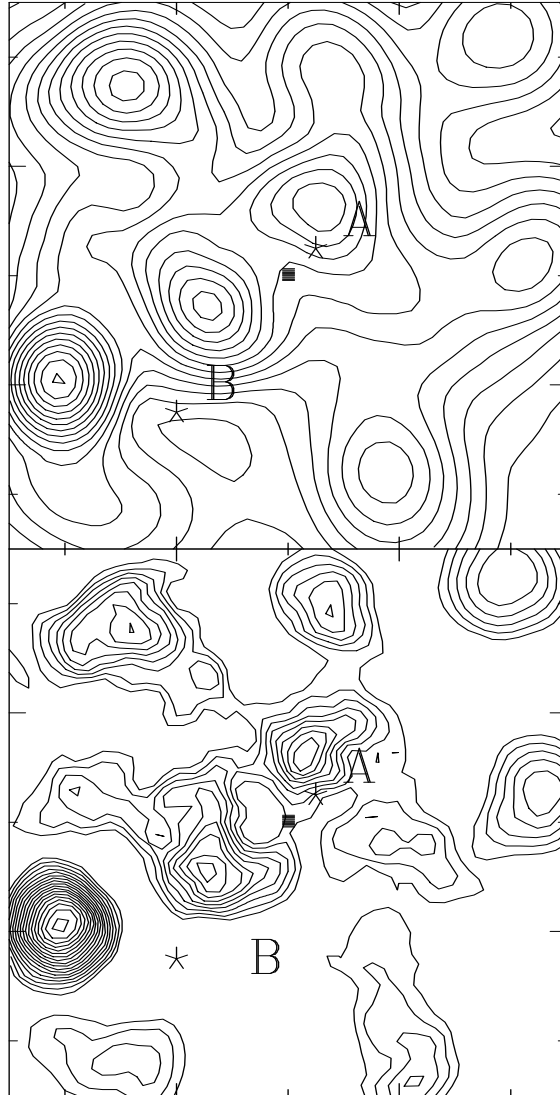


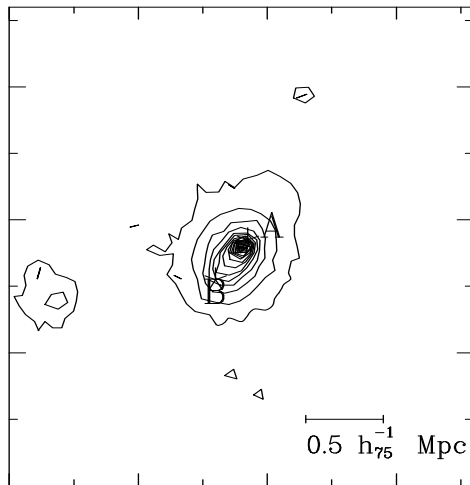
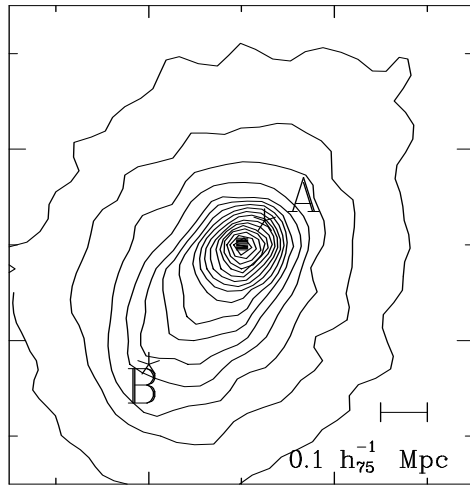
$0.1 h_{75}^{-1} \text{ Mpc}$

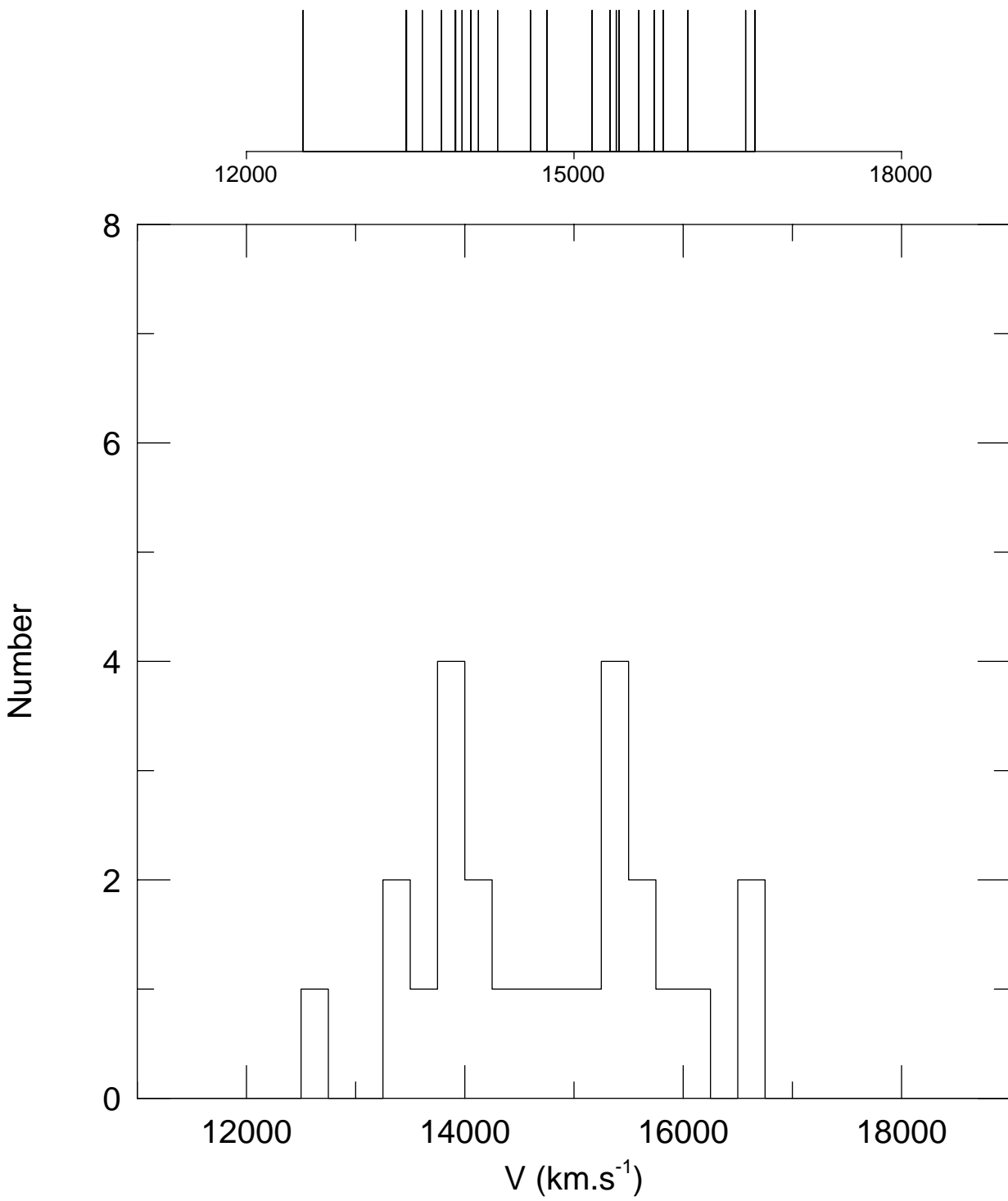




$0.1 h_{75}^{-1} \text{ Mpc}$

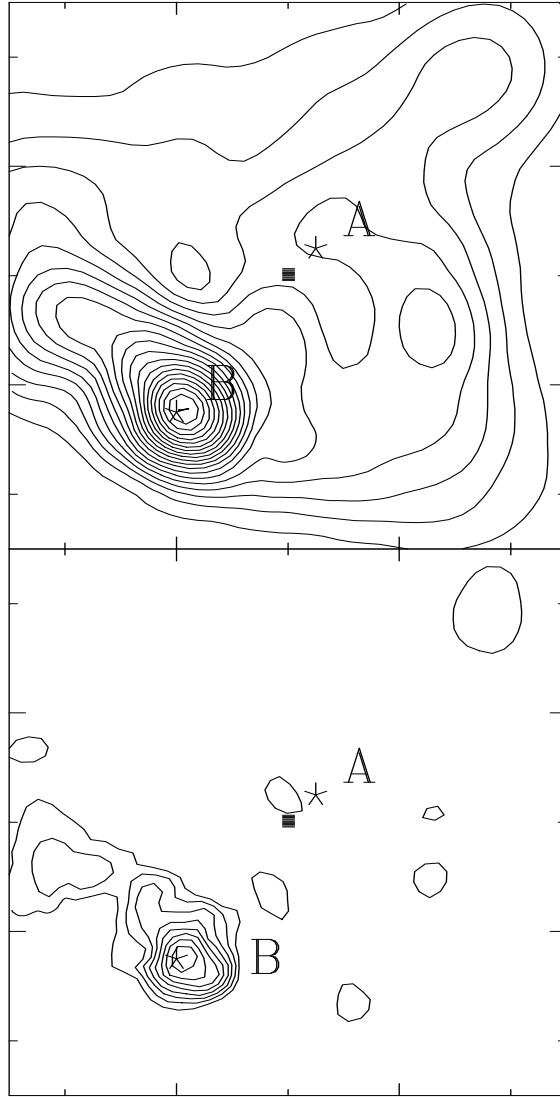








$0.1 h_{75}^{-1} \text{ Mpc}$



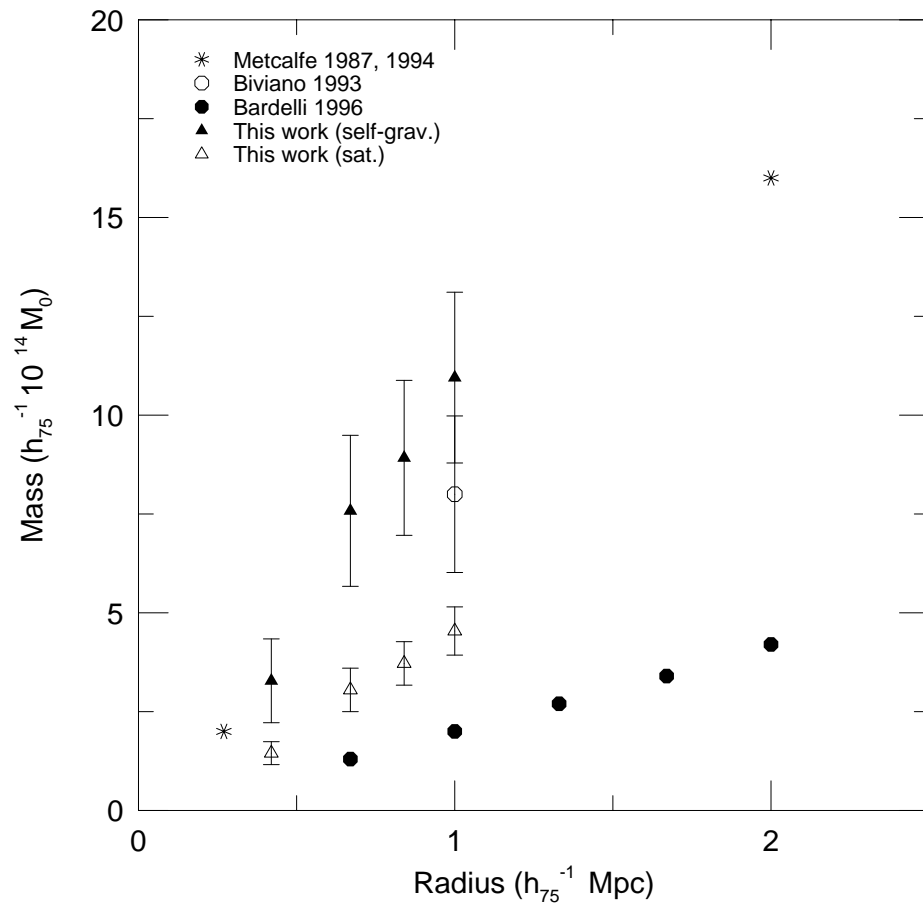


Table 1. Probability of galaxy classification in given resolution class

ΔB	$P(s g)$	$P(sf g)$	$P(g g)$	$P(d g)$	$P(long g)$
14-18	1 %	0 %	98 %	0.5 %	0 %
18-21	1 %	12 %	86 %	0 %	1 %

Table 2. Global kinematical parameters of major structures in the field around A3558

SAMPLE	C_{BI}	S_{BI}	N_{gal}	REF.
A3558	14434 (14377, 14492)	1030 (987, 1074)	282	This work
	14242 (14162, 14322)	986 (926, 1046)	150	Bardelli et al. 1996
	14233 (14142, 14324)	973 (913, 1102)	114	Teague et al. 1990
	14306 (14141, 14491)	923 (821, 1043)	80	Bird 1994
	14237 (14087, 14387)	991 (834, 1148)	50	Metcalf et al.1987
	14628 (14478, 14778)	1044 (882, 1342)	13	Melnick & Quintana 1981
$R < 900$ arcsec	14238 (14144, 14331)	1016 (952, 1079)	133	This work
SC1327-312	14841 (14701, 14980)	580 (462,699)	16	This work

Table 3. Structure characteristics and kinematical parameters of the central core region substructures

Structure	N_{gal}	C_{BI}	S_{BI}
A	24	14732 (14501,14963)	1142(1002,1283)
A'	13	15565 (15389, 15741)	587 (442,731)
B	25	14012 (13855,14169)	897 (781,1012)
core - A'	65	14022 (13919, 14125)	769 (697,841)
core - A' - B	40	14035 (13922, 14148)	683 (587,779)

Table 4.

Structure	Radius	N_{gal}	C_{BI}	S_{BI}	$M_{selfgrav}$	M_{sat}	M_{sat}/L
$R < 500''$	0.42	59	14046 (13940,14152)	806 (726,886)	3.28 (1.06)	1.45 (0.29)	0.25 (0.05)
$R < 798''$	0.67	98	14065 (13966,14165)	978 (913,1042)	7.58 (1.91)	3.05 (0.55)	0.27 (0.05)
$R < 1000''$	0.84	130	14073 (13985,14161)	957 (903,1011)	8.91 (1.95)	3.72 (0.55)	0.24 (0.04)
$R < 1200''$	1.00	160	14160 (14081,14243)	973 (924,1022)	10.95 (2.16)	4.53 (0.61)	0.23 (0.03)
SC1327-312	0.34	16	14841 (14701,14980)	580 (462,699)	1.07 (0.66)	0.38 (0.17)	0.21 (0.09)